applied optics

Optimization design of an ultralight large-aperture space mirror

Hao Wang,[1,2,*] Jiang Guo,[1] MingDong Shao,[1] JiMing Sun,[1] FuXiang Tian,[1] and Xu Yang[3]

[1]Changchun Institute of Optics, Fine Mechanics and Physics, Chinese Academy of Sciences, Changchun, 130033, China
[2]University of Chinese Academy of Sciences, Beijing 100049, China
[3]School of Mechanical and Aerospace Engineering, Jilin University, Changchun 130025, China
*Corresponding author: hit_hw@126.com

Received 11 October 2021; revised 17 November 2021; accepted 18 November 2021; posted 18 November 2021; published 8 December 2021

The ultralight space mirror has long been a hot topic in the research field of space telescopes. In this paper, an ultralight mirror is designed by obtaining the structure and parameters of a mirror with an aperture of 2 m through experimental design and multiobjective integrated optimization. Specifically, the materials near the neutral surface were replaced with elliptical holes. The back of the mirror was supported at three points. Finite-element analysis shows that the mirror had a surface figure error of 10.4 nm under 1 g in the *x* direction (gravity direction), which is sufficiently high to be applied to visible light optical systems. Further, the eigenfrequencies of mirror components were obtained through finite-element analysis: 70 Hz in the *x* direction, 70 Hz in the *y* direction, and 90 Hz in the *z* direction. The results demonstrate the excellent dynamics performance of the designed mirror. Compared with test results, the relative error of eigenfrequencies was within 4%. Hence, our ultralight design outputs reliable optimization results and applies to the development of large-aperture ultralight space mirrors. Finally, the ultralight mirror was prepared from reaction-bonded silicon carbide. The mass and surface density of the prepared mirror were 105 kg and 34 kg/m^2, respectively. The mirror mass was 50% lighter than that of the mirrors designed by traditional lightweight methods.

https://doi.org/10.1364/AO.445384

1. INTRODUCTION

The current research on large-aperture mirrors mainly focuses on traditional lightweight mirrors. Using a traditional empirical formula, Zhai Yan *et al*. [1] carried out lightweight design of a Φ2020 mm silicon carbide (SiC) infrared primary mirror. The model weight is 228 kg, and the surface density is 70 kg/m^2. Wang Kejun *et al*. [2] followed traditional empirical design to develop a Φ2000 mm SiC space mirror, with a substrate weight of 326 kg and a surface density of 103.8 kg/m^2. Gaia [3], a space observatory of the European Space Agency (ESA), consists of two infrared off-axis space telescopes. The primary mirror is a 1500 mm × 650 mm ultralight SiC mirror, whose weight is 38 kg and surface density is 39 kg/m^2. The Stratospheric Observatory for Infrared Astronomy (SOPHIA), a joint project of The National Aeronautics and Space Administration (NASA) and German Space Agency, features an infrared space telescope with a diameter of 2.7 m and a weight of 850 kg [4]. The famous Hubble Space Telescope has an aperture of 2.4 m and a weight of 890 kg. Its surface figure error meets the imaging requirement [5]. Hilpert *et al*. [6] manufactured a lightweight mirror by selective laser melting; the optimized lightweight mirror exhibits 63.5% of mass reduction and a higher stiffness compared to conventional designs. Lemared *et al*. [7] proposed a new way to manufacture large lightweight aspherics for space telescopes using stress mirror polishing (SMP). Atkins *et al*. [8] manufactured lightweight mirrors with a complex structure using a 3D print. Zhang *et al*. [9] designed a Φ510 mm mirror blank with weight about 2.2 kg. Table 1 shows the main parameters of large-aperture mirror in the literature.

Table 1. Main Parameters of Large-Aperture Mirror in the Literature

Parameter	Diameter (mm)	Mass (kg/m^2)	Working Ranges
[1]	Φ2020	70	IR
[2]	Φ2000	103.8	visible
Gaia	1500 × 650	39	IR
SOPHIA	Φ2700	148	IR
HST	Φ2400	196	visible
JWST	Φ6500	20	IR
Herschel	Φ3500	21	IR

The above analysis shows that most large-aperture space mirrors are relatively heavy. The high-mass mirrors increase the weight of the entire space telescope system. In the James Webb Space Telescope (JWST) and the William Herschel Telescope, the extra-large-aperture primary mirrors only apply to infrared

optical systems with a low requirement on surface figure error, despite their ultralow surface density [10,11].

Therefore, it is of great significance to develop lightweight large-aperture space mirrors with a high rigidity and a high surface figure error. This paper designs an ultralight mirror with an aperture of 2 m through experimental design and multiobjective integrated optimization. The designed mirror simultaneously achieves light weight, high rigidity, and high surface accuracy.

2. OPTIMIZATION DESIGN OF MIRROR

A. Structural Optimization

The lightweight mirror design essentially removes excess materials, retaining the useful parts. After the removal, the back of the mirror becomes porous. In general, there are five basic structural forms of the back: the symmetric interlayer, the asymmetric interlayer, the semi-open structure, the open structure, and the foam sandwich. The ribs are normally distributed in three forms, namely, triangular, hexagonal, and fan-shaped [12].

Suppose the aperture (D_o), center hole (D_i), and spherical parameters are determined for the target mirror. This paper designs the mirror in the following steps: determining structural form, selecting materials, optimizing structural parameters, and calculating results. The semi-open triangular structure was adopted for the back of the mirror, or its high rigidity and high stability. Figure 1 presents the optimization results through experimental design. The directions of the x and y axes are specified in Fig. 1(b). The z axis follows the Cartesian coordinate system, which is adopted in the subsequent discussion.

It is worth mentioning that, during structural optimization, the location of mounting holes was determined indirectly through the planning of vertical ribs, in order to ensure the mounting holes were under uniform stress. The mounting holes were arranged at the intersections of the main ribs. To facilitate the preparation, the vertical ribs were bent to converge at one point [indicated by green arrows in Fig. 1(b)].

Considering the limited contribution of the materials near the neutral surface to the bending rigidity of the mirror, these materials were replaced with elliptical holes. After the replacement, the mirror mass was reduced by 10%. During the simulation on rectangular holes, it was learned that this structure can reduce the mirror mass to the maximum degree, but the mirror with rectangular holes has a smaller surface figure error than that with elliptical holes. The reason is that the elliptical holes do not weaken the strength of rib intersections. The mirror mass can be reduced without sacrificing much of the rigidity. Figures 2(a) and 2(b) shows two kinds of mirror structure in the same mirror parameter case. Through finite-element analysis,

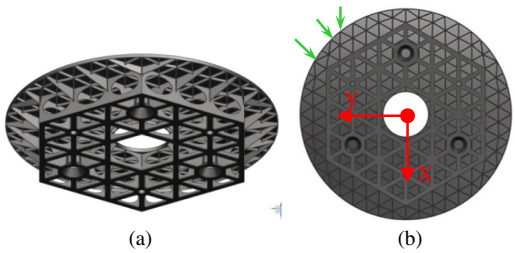

Fig. 1. Ultralight mirror model. (a) Model axonometric drawing; (b) model front view.

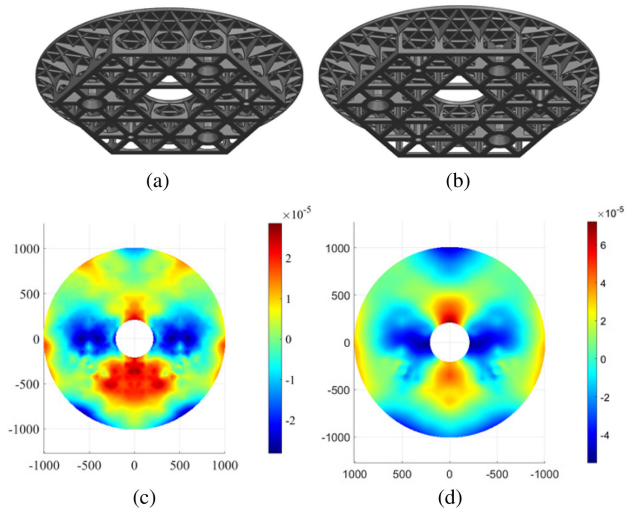

Fig. 2. Rectangle and elliptical holes' result of comparison. (a) Ultralight mirror mode of elliptical holes; (b) ultralight mirror mode of rectangle holes; (c) elliptical holes' surface figure error map of the mirror; (d) rectangular holes' surface figure error map of the mirror.

Table 2. Mirror Surface Figure Error of Elliptical Holes and Rectangular Holes

Parameter	Elliptical Holes	Rectangular Holes
RMS-X (nm)	10.4	20.3
Mass (kg)	103	100

Figs. 2(c) and 2(d) show the rectangle and elliptical holes' surface figure error map of the mirror. Table 2 shows that the surface figure error of the elliptical holes is better than that of the rectangular holes, but the elliptical holes are easier to manufacture, so elliptical holes were used.

B. Selection of Mirror Materials

Table 3 shows common materials for a spaceborne mirror. Comparing SiC with other materials such as ULE, Zerodur, and Be, SiC is the most suitable material for developing our mirror, which is characterized by a complex structure. SiC is an ideal optical material for space mirrors, thanks to its large specific rigidity, good thermal conductivity, and small coefficient of linear expansion. Depending on preparation technique, SiC can be divided into several types. Those commonly used in mirrors include hot-pressed SiC (HP-SiC), reaction-bonded SiC (RB-SiC), pressureless-sintered SiC (S-SiC), and chemical vapor decomposition SiC (CVD-SiC). Among them, RB-SiC boasts a low sintering temperature, a small production cost, and a high degree of material densification. Most importantly, this SiC material does not undergo volume contraction, providing a desired material for the preparation of large complex-shaped structural members [13,14]. The author's employer (Changchun Institute of Optics, Fine Mechanics and Physics, Chinese Academy of Sciences) has excellent fabrication capacity for RB-SiC. In 2018, a Φ4Φ4 m mirror was prepared [15]. Mirror blanks with high lightness, high rigidity, and complex structure can be manufactured in a short time. Therefore, RB-SiC was selected as the 2 m ultralight mirror material.

Table 3. Values of Material Properties for Common Spaceborne Mirror Material

Material	SiC	Be	ULE	Zerodur
Density ρ (g/cm^3)	3.0	1.85	2.21	2.53
Young 's modulus E (Gpa)	350	287	67	92
Thermal cond. λ (W/m · K)	144	216	1.3	1.46
CTE α (ppm/K at RK)	2.4	11.3	0.015	0.02
Mechanical stability (E/ρ)	116.67	155.14	30.2	36.36
Thermal stability (λ/α)	60	19.12	86.67	73
Integrated performance (E/ρ). (λ/α)	7000	2966	2654	2627

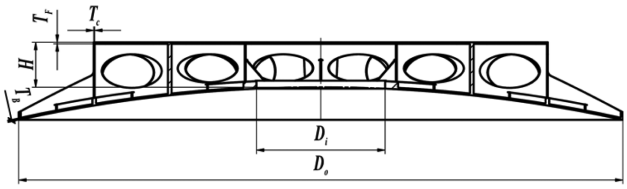

Fig. 3. Dimensional parameters of the mirror.

C. Multiobjective Integrated Optimization of Mirror

The structure of the ultralight mirror was optimized through experimental design. After that, the optimization aims to select the best structural parameters. The surface figure error of the mirror is not simply the results of superposition of structural parameters. The key to mirror design is to quickly find the optimal solution. In traditional design, iterative computation is performed with empirical formulas to obtain an acceptable outcome. But the traditional approach is very likely to converge to a set of local optimal solutions. The design process is inefficient, and it is difficult to obtain the optimal solution. This paper resorts to the highly efficient multiobjective integrated optimization to find the best parameters for the mirror.

D. Parameter Optimization

For a given optical system, many parameters for the mirror have fixed values, such as spherical radius, center hole, and aperture. These parameters were therefore excluded from the optimization problem. As shown in Fig. 3, the following parameters for the back of the mirror need to be optimized: mirror thickness T_B, center height H, back plane thickness T_F, and rear panel thickness Tc.

E. Optimization Model

The optimization design for the ultralight mirror aims to find a set of optimal parameters, such that the surface figure error RMS_X of mirror X is greater than $1/50\lambda(\lambda = 632.8\,\text{nm})$, the fundamental frequency (f) is above 80 Hz, and the mass is below 124 kg. For simplicity, the eigenfrequencies were taken as a constraint, reducing the number of objective functions from three to two. In essence, the optimization problem is to search for the set of Pareto optimal solutions to the two remaining objective functions. During the optimization process, the fundamental frequency (f) of the mirror was calculated and

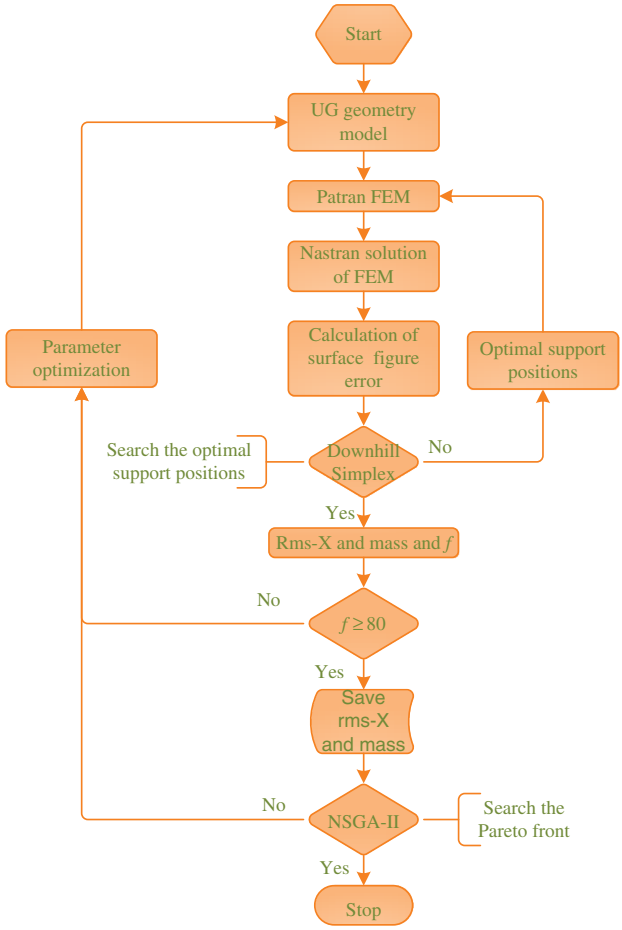

Fig. 4. Flow chart of integrated optimization.

compared with the condition of 80 Hz. The mirror is fixed with three flexures, and its properties are similar to kinematic constraints. This flexure does not affect the optimization result of the entire structure. It can realize the decoupling of the flexures structure and the mirror structure. This support does not affect the optimization result of the entire structure. The range of each parameter can be determined by the current manufacturing capability. Then, the optimization model can be mathematically described as

$$\begin{cases} \text{find}(X) = (T_B,\ T_F,\ T_C,\ H)^T \\ \min(\text{RMS\_X},\ \text{Mass}) \\ S.T \\ 3 \le T_B \le 6 \\ 2.5 \le T_F \le 10 \\ 3 \le T_C \le 8 \\ 120 \le H \le 200 \\ 80 \le f \end{cases}.$$

Figure 4 presents the flow of integrated optimization. Specifically, Unigraphics (UG) was adopted to establish the geometry model after experimental design, Patran was selected as the finite-element model (FEM), Nastran was chosen to compute the surface figure error of the mirror, and nondomination-based genetic algorithm (NSGA-II) was called to search for the global solution set.

Table 4. NSGA II Parameters

Parameter	Value
Population size	12
Number of generations	20
Crossover probability	0.9
Crossover distribution index	10
Mutation distribution index	20

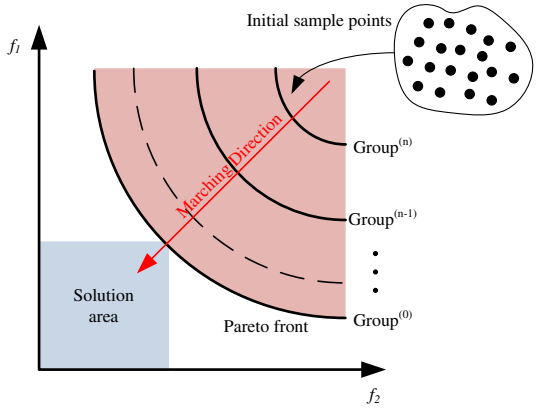

Fig. 5. Principle of approaching Pareto front step by step.

In our design, many mirror parameters are coupled with each other, pushing up the computing load. Thus, a suitable optimization algorithm needs to be selected to obtain the solution set of the objective functions. Here, NSGA-II [16] is employed for its excellent search performance. Table 4 shows the parameter setting of NSGA-II, which quickly converges to precise solutions. NSGA-II is one of the nonscalar methods. It can make the front of the solution set close to the Pareto front as much as possible, and try to cover the Pareto front evenly. Figure 5 shows the process of calculation. The initial solution value was used as starting point-group (n), and then gradually improved in order: $\text{group}^{(n)} \rightarrow \text{grou}^{p(n-1)} \rightarrow \ldots \rightarrow \text{group}^{(1)} \rightarrow \text{group}^{(0)}$, approaching the real Pareto front. In addition, downhill simplex was called to directly search the optimal support positions. Next, the RMS_X and weight were calculated based on the optimal support positions. The two optimization objectives, namely, RMS and mass, are recorded in units of nanometers and kilograms, and assigned weights of 10 and 1, respectively.

F. Optimization Process

During the optimization, it was learned that the results were mostly significantly affected by the T_C and T_B of the mirror. After 118 iterations, T_C converged to 3.05 mm, and T_B also converged to that level. Meanwhile, H and T_F oscillated about the optimal values. Figure 6 shows the trends obtained through polynomial fitting.

3. RESULTS

The above optimization outputs the Pareto solution sets of mirror mass and RMS_X. As shown in Fig. 7, the results gradually approached the lower-left corner, forming a boundary called the Pareto frontier. To ensure the allowance for machining,

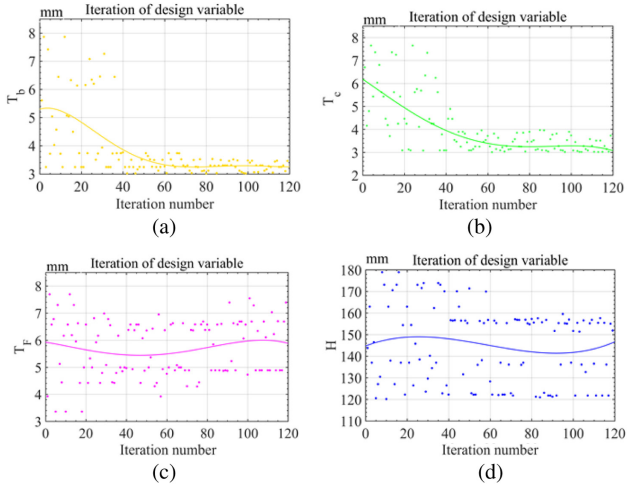

Fig. 6. Iterative curves of size parameters. (a) Parameter T_B, (b) parameter T_C, (c) parameter T_F, (d) parameter T_B.

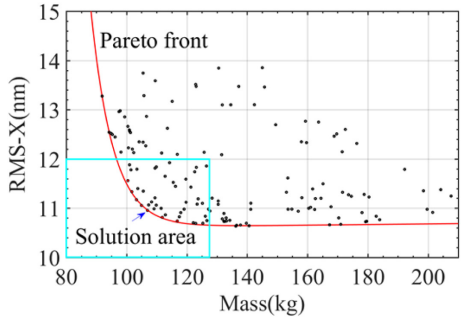

Fig. 7. Pareto solution sets of mirror mass and RMS_X.

Table 5. Final Results of Parameter Optimization

Target Parameter	Optimized Value (mm)	Machining Precision (mm)
T_B	3.05	3
T_F	6.1	6
H	151.33	150
T_C	3.05	3

the point in the set of effective solutions, which is the closest to the lower-left corner, was taken as the final solution (indicated by the blue arrow), and rounded to obtain the precise dimensions (Table 5). The elliptical holes dimension (the long axis is 200 mm and the short axis is 112 mm) were determined after the mirror parameters optimization was completed, in order to simplify the optimization model and reduce the amount of calculation. Then, the final geometry model was established based on the precise dimensions (Fig. 1). The final mirror model has a mass of 103 kg. To validate the optimization results, a finite-element analysis was performed on the statics and dynamics features of the ultralight mirror.

A. Statics Analysis

The optical axis direction of the large-aperture mirror in ground processing differs from that in testing. The optical axis is vertical

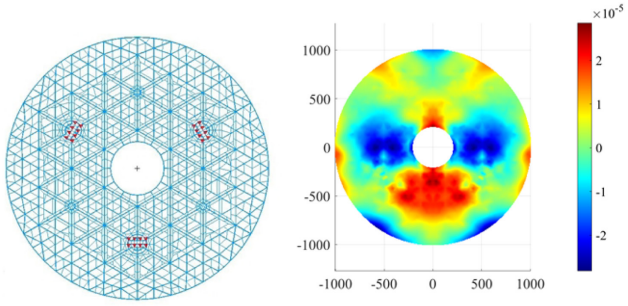

(a) (b)

Fig. 8. FEM results. (a) Under FEM constraint of 1 g; (b) surface figure error map of the mirror.

Table 6. Mirror Surface Shape Data under 1 g[a]

ΔX (μm)	ΔY (μm)	ΔZ (μm)	Θx (″)	Θy (″)	Θz (″)	PV (nm)	RMS_X (nm)
0.2	38.7	−0.1	0.3	−0.1	≈0	61.2	10.4

[a]ΔX, ΔY, and ΔZ are rigid body displacements; θx, θy, and θz are dip angles of the mirror.

during ground processing and horizontal during testing. The mirror belongs to two different force states under the two conditions, owing to the gravity of the ground. If the statics state of the mirror fails to meet the testing requirement, i.e., the surface figure error of the mirror with horizontal optical axis surpasses allowable RMS_X by 1/50λ (λ = 632.8 nm), the mirror structure will undergo the gravity deflection that will go away in the weightless environment of space. The surface figure error will be altered, dragging down the imaging quality of the optical system. Hence, under the gravity of 1 g, the surface figure error of the mirror with horizontal optical axis on the ground must be better than 1/50λ (λ = 632.8 nm). According to the boundary conditions (horizontal optical axis; 1 g of gravity in the x direction), the back support was exact-constrained by three flexures; the flexure interfaces [Fig. 8(a)] were fixed-constrained. Then, the surface figure error of the mirror model was subjected to finite-element analysis. The results show that the mirror had an RMS_X of 10.4 nm [surface shape distribution in Fig. 8(b)]; analysis results in Table 6), i.e., the statics features of the mirror meet the design requirements.

B. Dynamics Analysis and Test

During the launch and flight, the space mirror needs to go through a complex dynamics environment. The dynamics analysis on a large-aperture space mirror helps to predict whether the response of the mirror structure to vibration and impact load meets the strength requirement, and whether the materials of the space mirror could be damaged. Here, an eigenfrequencies analysis were conducted on the mirror component model (the mirror and the flexure and the supporting frame), and a feature scan was applied on the mirror components. Figure 9 shows the mirror component was fixed on the shaker through the fixture for vibration tests. The mirror component was excited by the shaker. Under the test conditions (Table 7), the eigenfrequencies of the mirror components were measured in three directions. Figure 10 shows the mounting position of

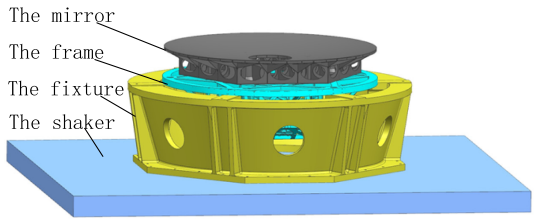

Fig. 9. Schematic diagram of vibration tests.

Table 7. Feature Scan Test Conditions (X, Y, Z)

Frequency Range (Hz)	Amplitude (g)	Scan Frequency (oct/min)
8–500	0.1	4

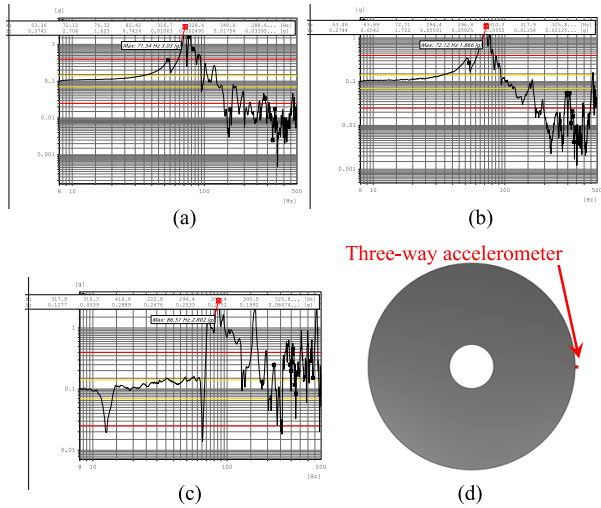

Fig. 10. Test results. (a) Test results on x directions; (b) test results on y directions; (c) test results on z directions; (d) mounting position of the three-way accelerometer.

Table 8. Comparison between Simulation Results and Test Results

Direction	X	Y	Z
Finite-element analysis eigenfrequencies (Hz)	70	70	90
Test eigenfrequencies (Hz)	71.54	72.12	86.51
Relative error (%)	2.1	2.9	4

the three-way accelerometer and the test results. It can be seen that the mirror exhibited good dynamics performance. Table 8 presents the finite-element analysis results and test results. The error between the two sets of results was within 4%, which indirectly demonstrates the reasonability of our optimization method.

The above analysis confirms that our mirror satisfies engineering requirements. The mirror of the designed structural dimensions was prepared through reaction bonding. The mass and surface densities were 105 kg and 34 kg/m^2, respectively. As shown in Table 9, our mirror was 50% lighter than the mirrors with the same aperture reported in the literature.

Table 9. Performance Comparison between Mirrors with the Same Aperture Reported in the Literature

Aperture (mm)	Φ2020 (our design)	Φ2020 [1]	Φ2000 [2]
Mass (kg)	105	228	326
Surface density (kg/m^2)	34	70	103.8
Material	RB-SiC	SiC	RB-SiC
Surface figure error (RMS) (nm)	10.4	27.02	4.3

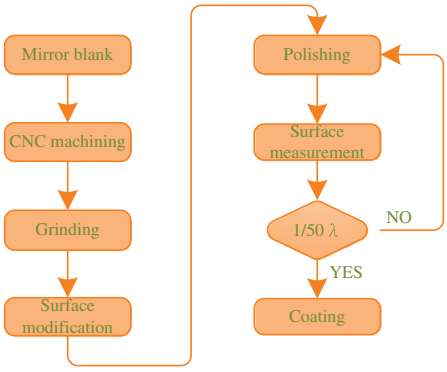

Fig. 11. Flow chart of the mirror's manufacturing.

C. Mirror Manufacturing Process

Figure 11 shows the mirror manufacturing process. The mirror combines with lost foam and improved gel-casting technologies; an RB-SiC mirror blank with monolithic partially closed back structure is produced, further improving the RB-SiC mirror's stiffness. The largest in the world, Φ4.0 m lightweight RB-SiC optical mirror blank is fabricated [17]. Due to high flexural strength (larger than 25 MPa), the mirror mounting holes have been machined by a computerized numerically controlled (CNC) process. While the surface figure error was ground to 2λ(λ = 632.8 nm), in order to eliminate the surface microdefect after the direct polishing of RB-SiC substrate, reduce the surface roughness, and increase the surface quality, Si was selected as the modified material based on the features of large-aperture SiC, where the mirror substrate was modified by using the magnetron sputtering technology [18,19]. Finally, while the surface figure error is polished to 1/50λ(λ = 632.8 nm) [20,21], the mirror surface will be coated. As shown in Fig. 12, the mirror is polished, and its surface figure error is 67 nm with a horizontal optical axis.

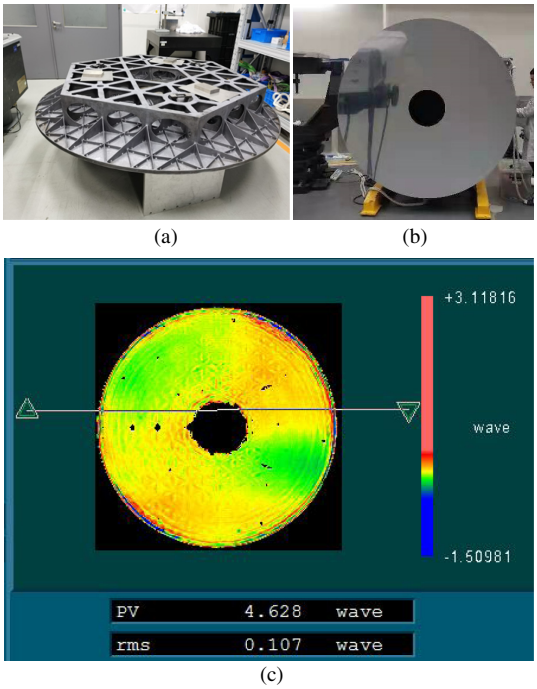

(a) (b) (c)

Fig. 12. Physical mirror. (a) Support mounting diagram, (b) mirror surface testing process, (c) interferometer detection results.

4. CONCLUSIONS

This paper optimizes mirror structure through experimental design and obtains mirror parameters through multiobjective integrated optimization, thereby designing an ultralight large-aperture mirror for space telescopes. The NSGA-II algorithm was called to improve the calculation efficiency during the construction of the multiobjective integrated optimization model. In addition, a geometry model was established for the mirror according to precise dimensions and used to analyze the statics and dynamics features of the mirror. Furthermore, the eigenfrequencies of the mirror components were tested, and the analysis data were contrasted with the test data. The relative error of eigenfrequencies was within 4%, reflecting the accuracy and practicality of our design approach. Finally, a physical mirror was prepared based on the designed structure and parameters. The mass and surface densities were 105 kg and 34 kg/m^2, respectively. The mirror mass was 50% lighter than that of the mirrors designed by traditional lightweight methods. Currently, the mirror is in the stage of precision optical processing, and its surface figure error is 67 nm with a horizontal optical axis.

Acknowledgment. This work is supported by the Changchun Institute of Optics, Fine Mechanics and Physics Innovation Project.

Disclosures. The authors declare no conflicts of interest.

Data Availability. Data underlying the results presented in this paper are not publicly available at this time but may be obtained from the authors upon reasonable request.

REFERENCES

1. Y. Zhai, G. Mei, F. Jiang, and P. Qian-Shuai, "Φ2 020 mm aperture space infrared camera main reflector design," Chin. J. Lumin. **39**, 1170–1176 (2018).
2. K. Wang and J. Dong, "Structural design of Φ2 m-level large-diameter SiC reflector used in space remote sensor," Infrared Laser Eng. **46**, 718005 (2017).
3. M. Bougoin and J. Lavenac, "From Herschel to Gaia: 3-meter class SiC space optics," Proc. SPIE **8126**, 50–58 (2011).
4. J. Billet, "SOFIA lightweight primary mirror," Proc. SPIE **3352**, 354–365 (1998).
5. L. A. Montagnino, "Test and evaluation of the Hubble space telescope 2.4-meter primary mirror," Proc. SPIE **571**, 182–190 (1986).
6. E. Hilpert, J. Hartung, S. Risse, R. Eberhardt, and A. Tünnermann, "Precision manufacturing of a lightweight mirror body made by selective laser melting," Precis. Eng. **53**, 310–317 (2018).

7. S. Lemared, M. Ferrari, C. D. Jeu, T. Dufour, N. Soulier, and E. Hugot, "Stress mirror polishing for future large lightweight mirrors: design using shape optimization," Opt. Express **28**, 14055–14071 (2020).
8. C. Atkins, C. Feldman, D. Brooks, S. Watson, W. Cochrane, M. Roulet, E. Hugot, M. Beardsley, M. Harris, C. Spindloe, and S. G. Alcock, "Topological design of lightweight additively manufactured mirrors for space," Proc. SPIE **10706**, 107060I (2018).
9. Y. Y. Zhang, W. Jing, Y. T. Cheng, H. U. Gui-Tao, and J. Z. Fang, "Design and finite element analysis of Φ510 mm SiC ultra-lightweight mirror," Opt. Precis. Eng. **20**, 1718–1724 (2012).
10. H. P. Stahl, "JWST primary mirror technology development lessons learned," Proc. SPIE **7796**, 779604 (2010).
11. Y. Toulemont, T. Passvogel, G. L. Pilbratt, D. D. Chambure, D. Pierot, and D. Castel, "The 3.5-m all-SiC telescope for HERSCHEL," Proc. SPIE **5487**, 1119–1128 (2004).
12. P. Yoder and D. Vukobratovich, *Opto-Mechanical Systems Design*, 4th ed. (CRC Press, 2015).
13. Z. Ge, Z. Ru-Cheng, and Z. Wen-Xing, "Fabrication and test of large scale light-weight SiC mirror," Opt. Precis. Eng. **14**, 759–763 (2006).
14. J. Guo, "Research on design an manufacturing of large aperture space mirror of silicon carbide," Ph.D. diss. (Jilin University, 2019).
15. H. U. Hai-Fei, Z. Hong-Wei, L. Zhen-Yu, L. Xiao, and Z. Xue-Jun, "Hydrostatic support system for in-situ optical testing of a 4 m aperture SiC mirror," Guangxue Jingmi Gongcheng/Opt. Precis. Eng. **25**, 2607–2613 (2017).
16. K. Deb, A. Pratap, S. Agarwal, and T. Meyarivan, "A fast and elitist multiobjective genetic algorithm: NSGA-II," IEEE Trans. Evol. Comput. **6**, 182–197 (2002).
17. G. Zhang, C. Cui, B. Dong, Q. Cao, and J. Bao, "Fabricating of Φ4m CIOMP-SiC mirror blank," Proc. SPIE **10837**, 108370I (2019).
18. X. Ling, L. Xiao, L. Zhenyu, Z. Ligong, Z. Feng, and Z. Xuejun, "Measurement of 2 m SiC asphere mirror based on swing arm profilometer," Acta Opt. Sin. **35**, 1212002 (2015).
19. Z. Liu, J. S. Gao, and H. Liu, "Surface modification of 2 m RB-SiC substrate by magnetron sputtering," Opt. Precis. Eng. **24**, 1557–1563 (2016).
20. L. Yi, X. Zhang, H. Hu, Z. Zhang, and G. E. Zhang, "Equivalent thin-plate method for stressed mirror polishing of an off-axis aspheric silicon carbide lightweight mirror," Opt. Express **28**, 36413–36431 (2020).
21. L. Li, Z. Liu, D. Xue, W. Deng, R. Li, Y. Bai, X. Zeng, and X. Zhang, "Rapid fabrication of a lightweight 2 m reaction-bonded SiC aspherical mirror," Results Phys. **10**, 903–912 (2018).